COST ACTION FP 1402

"Basis of Structural Timber Design :
From Research to Standards"

Report on Short Term Scientific Mission
for Project Entitled

Simplified Modelling for Multi-Span Continuous Timber-Concrete Composite Floors

ECOST-STSM-FP1402-130316-070799

by

Wendel Sebastian – MA (Cantab), PhD (Cantab)

Queen's School of Engineering, University of Bristol, UK

This report describes collaborative research conducted between 13th and 27th March 2016.

Host : Professor Alfredo Manuel Pereira Geraldes Dias, Departamento de Engenharia Civil – FCTUC, University of Coimbra, Portugal.

Table of Contents

1 - Introduction

Timber-concrete composite (TCC) floors comprise thin concrete slabs shear connected to timber joists. TCC floors combine the low carbon footprint and sustainability of responsibly sourced timber with the higher stiffness, thermal mass, fire resistance and acoustic insulation of concrete. The low-density joists and thin slabs enable much lighter and cheaper building foundations than do all-concrete floors. Relative to all-timber floors the concrete lowers energy bills, deflections and vibrations, and improves strength, fire resistance and acoustic insulation. TCCs can improve the structural integrity of floors in historic buildings by casting and connecting concrete slabs onto the existing joists with the floorboards used as formwork, or they may be part of new buildings where they serve in the dual role of floors and diaphragms against wind or seismic loads.

Notable new-build applications of TCC floors include the 8-storey Life Cycle Tower One (LCT1) office building in Dornbirn (2012, Austria), the Earth Sciences Building at the University of British Columbia (2013, Canada), and the Dr Chau Chak Wing building designed by celebrated architect Frank Gehry for the University of Technology Sydney (2014, Australia). Use of prefabricated TCC panels contributed to rapid rise of the LCT1 at the rate of one storey per day.

The load responses of TCC floors can be nonlinearly influenced by factors including:

- Statical indeterminacy of the TCC system.
- The nonlinear shear force vs slip characteristics of the connections.
- Cracking or compression softening of the concrete.
- Possible yield of the slab's steel reinforcement.
- Compression softening of the timber.

Indeterminacy affects load response by influencing stress redistribution globally or locally, depending on whether the indeterminacy is external or internal, as follows:

- *Internal* indeterminacy (InI) owes its existence to the slab-joist interface slip. Thus it occurs *within* the TCC member and affects the way in which a moment on the composite T-section is shared between the slab and the beam.
- *Longitudinal external* indeterminacy, or LEI, occurs for multi-span continuous TCC members due to the moment transfers across the multiple supports in the

longitudinal direction. It arises because the number of supports exceeds the number of global equilibrium equations which can be written for the TCC assembly. For any given load on the structure, this form of indeterminacy influences the moment distribution along the entire length of the member.

- *Transverse external* indeterminacy, or TEI, occurs for TCCs with multiple longitudinal joists spaced transversely. It is parasitic on the transverse stiffness of the slab, and influences transverse distribution of both joist reactions at any support and TCC-section moments across any full width of the assembly.

Research to date (e.g. [1-6]) has elucidated the load responses of single joist, simply supported TCCs, which exhibit only InI. In practice TCC floors to date have also been single span simply supported, but with multiple parallel joists, so they exhibit both InI and TEI, giving rise to more complex behaviour. Despite this, few studies (e.g. Dias et. al. [7], Kieslich & Holschemacher [8]) have addressed real TCC floors.

If instead the multi-joist TCC assembly is also multi-span continuous longitudinally, then all three forms of indeterminacy co-exist. The longitudinal continuity can be exploited to reduce deflections and enhance load capacity. This is an area in which fundamental research is needed. To that end a recent experimental study by Sebastian et. al. [9], in a collaborative venture between the Universities of Trento (Italy) and Bristol (UK), focused on the mechanics of multi-span continuous single T-section TCC beams, where InI and LEI were both present.

Due to the indeterminacy, any analysis aimed at predicting TCC load response must capture the spatial stiffness profile of the TCC assembly. This profile evolves under increasing load owing to progressive cracking and compression softening of the concrete in the longitudinal and transverse directions, and to compression and shear softenings respectively of the timber and connectors, both due to longitudinal bending. The above-described forms of indeterminacy will strongly accentuate nonlinear interaction between these longitudinal and transverse actions.

For user-friendliness in the design office, a beam element computer analysis is preferable. Hence this report presents a framework of ideas for determining the flexural stiffnesses – in a form compatible with beam element analysis – of TCC sections including the complex effects of slip and curvature. Test data from a uniquely instrumented TCC beam are used to verify key features of this framework.

2 – Basis of Analysis Approach

A fundamental premise of this work is that a TCC assembly comprises two main features, namely the timber-concrete composite section and the connections. Both these features must be explicitly modelled in analysing the TCC assembly under load. To that end, thus far there has been considerable investment in experimental research in particular, to establish the characteristics of the *connections*. By contrast, little published research exists on defining the TCC *section* properties.

Nonlinear FE (NLFE) analysis is a powerful tool for predicting the load responses of TCCs. Now in the NLFE approach, the slab and beam elements are typically separated by the connection elements. Hence the connections are explicitly represented, but the TCC section is not owing to its fragmentation into the slab and beam components. This limits physical appreciation of results from one of the most powerful current tools for nonlinear analysis of composite structures. Moreover, NLFE analysis is typically beyond the range of expertise available in design offices. Hence an analysis approach of comparable accuracy, which is readily usable in the design office, and which explicitly represents not only the connections but also the composite *section* in a non-fragmented manner, is desirable.

The gamma method of Eurocode 5 [10] provides a user-friendly approach to predicting TCC behaviour under load. However the method is limited to single span, simply supported, linear elastic beams under uniformly distributed loads. Other rigorous ultimate limit state analyses (e.g. [11]) have been presented which assume perfectly plastic (and hence nonlinear) behaviour of the connections, while the timber and concrete are assumed to be linear.

Hence there is a clear need to complement the status quo by introducing a means of accounting for the effects, at *composite section* level, of concrete cracking and compression softening, timber compression softening and possible steel yield. This new focus on section behaviour can then be combined with the existing approach for connection behaviour to predict TCC load response at both the serviceability and ultimate limit states.

3 – Layered Approach and Novel M - κ - ε_s Surface

A key novelty of this work is the derivation of nonlinear characteristics for the timber-concrete *composite section* as an entity in its own right. In so doing, note that stress-strain expressions for nonlinear behaviour of concrete and timber in compression may not readily have closed-form integrals. Hence, it is prudent to derive composite section behaviour as the cumulative effect of behaviours calculated at discrete points in the slab and joist. This justifies use of a layered approach, in which the overall composite section properties are the summed effects of those from thin horizontal slices juxtaposed through the section depth.

Commonly, say for reinforced concrete (RC) sections, the assumption of rigid bond is made at the steel-concrete interface. This leads to a moment-curvature plot which defines the RC section. However for TCC sections the slip strain at the timber-concrete interface can, along with the curvature, significantly influence section behaviour. Hence a complete description of the composite section behaviour entails moment as a function of both slip strain and section curvature.

In other words, the 2-D moment-curvature plot traditionally used for RC sections morphs into a (3-D) moment – slip strain – curvature **surface** for TCC sections. If moment, slip strain and curvature are denoted as M, κ and ε_s respectively, then this idea may be expressed as follows, namely :

$$f_1 (M, \kappa, \varepsilon_s) = 0 \qquad \text{Eqn 1}$$

In fact, as shown later in this report, the axial force (F) in either the beam or the slab section is also a function of curvature and slip strain and so leads to another surface which defines TCC section behaviour, as follows :

$$f_2 (F, \kappa, \varepsilon_s) = 0 \qquad \text{Eqn 2}$$

This is important, as axial equilibrium requires that the difference in the slab or joist axial force between two non-coincident sections along the beam equates to the

longitudinal shear force in the connection between those sections. Hence the (F , κ , ε_s) surface provides the basis of a means to relate the structural action of the composite section to that of the connections. Graphical representation (the surfaces) of these equations greatly facilitates visualisation of the spectrum of possible TCC section behaviours and so constitutes a desirable strength of this approach.

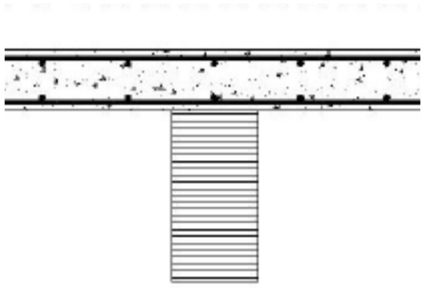

Fig. 1 – Generic TCC Section Considered in This Study

Fig. 1 shows the generic TCC section considered in the analyses. A core trio of variables are needed to define all possible section behaviours. These are the strain (ε_{ct}) at the top of the concrete slab, the slip strain (ε_s) at the slab-joist interface and the section curvature (κ). Full curvature compatibility is assumed between the slab and the joist, but note that this novel section analysis approach can equally cope with differential curvature between the slab and the joist.

Using this approach, the mid-depth strain for layer number k of the slab is as follows :

$$\varepsilon_{k,\,slab} = \varepsilon_{ct} - \kappa y_{k,\,slab} \qquad \text{Eqn 3}$$

Ditto the strain for any layer in the joist except now for the inclusion of the slip strain, as follows:

$$\varepsilon_{k,\,joist} = \varepsilon_{ct} + \varepsilon_s - \kappa y_{k,\,joist} \qquad \text{Eqn 4}$$

In both cases, y refers to the depth of the layer below the top of the slab. Sagging curvatures and compressive strains are positive.

Zero net axial force on the section is the governing equilibrium condition. In gravitating towards this condition, starting values were first assumed for two of the (ε_{ct}, κ, ε_s) trio of variables, and a guess was made for the corresponding value of the third variable. Once the details of the slab and joist layers were decided, then the values of $y_{k,\,slab}$ and $y_{k,\,joist}$ needed to calculate the strain at the centre of each layer consistent with Eqns 3 and 4 above were known. For each layer, after determining this strain, the relevant nonlinear constitutive model for the material of the layer was used to convert strain to stress, which was then converted to force for the layer assuming uniform distribution of stress over the area. Finally, the forces for all layers were summed. If this net force was non-zero, then a Newton-Raphson iterative scheme was used to nudge the computations in the direction of zero net force, as follows.

While any two of the (ε_{ct}, κ, ε_s) trio of variables could be used to start the computations, in this study starting values of ε_{ct} and κ were used, so that the objective was to find the corresponding value of ε_s which led to zero net axial force on the section. Taking the updated net axial force on the TCC section as F, the iterative process sought to reduce the force to zero by applying a $\Delta F = -F$ in the following context, namely :

$$\Delta F = \frac{\partial F}{\partial \varepsilon_s} \cdot \Delta \varepsilon_s \qquad \text{Eqn 5 ,}$$

where the partial differential is calculated by summing individual layer contributions. For a timber layer, this derivative is as follows, namely :

$$\frac{\partial F}{\partial \varepsilon_s} = \sum_{k,joist} \frac{\partial F_{k,joist}}{\partial \varepsilon_s} = \sum_{k,joist} \sigma'\left(\varepsilon_{k,joist}\right) \cdot A_{k,joist} \qquad \text{Eqn 6 ,}$$

where A_k is the area of layer k and $\sigma'(\varepsilon_{k,joist})$ is the derivative of stress with respect to strain for that layer, evaluated at the updated strain under consideration for that depth.

Owing to the nonlinearities embedded in the material constitutive models, a few iterations were needed for convergence (namely to achieve F = 0). On average fewer than 5 iterations were needed, with no more than 10 iterations having been required for any of the computations performed.

Once the condition of zero net axial on the entire TCC section had been achieved, the corresponding moment on the section was found by summing, across all layers, the product of axial force on each layer and the corresponding lever arm (vertical distance) from *any* reference point on or off the section to the centre of the layer. That this reference point can be arbitrary is a direct consequence of the zero net axial force on the section, because this leads to a unique section moment at the end of the computations, independently of the reference point. The important issue is that the *same* reference point is used for all layers in pursuing this computation. In the present study, this common point was taken as the top of the slab, since the vertical distance from this point to the centre of each layer was already available from the start of the computations.

A flowchart for these computations is provided in Fig. 2. F_{net} in the flowchart equates to F in Eqn 5, while the italicised *F* of Eqn 2 refers to the axial force in either the slab or joist (these two forces are equal and opposite at equilibrium of the section). As shown in the flowchart, for any given value of ε_{ct} , the value of κ was varied and the corresponding value of ε_s was found as above. This was done until some form of failure of the section (timber fracture in tension, timber crushing in compression, concrete crushing in compression) was found. At that stage the value of ε_{ct} was changed and the computations resumed. By this means the entire spectrum of behaviours possible for the composite section were found, enabling the (M , κ , ε_s) and (F , κ , ε_s) surfaces to be constructed.

Since the method is generic, both sagging and hogging curvatures could be represented in this scheme. The vast majority of studies to date have looked at sagging behaviour (single span, simply supported) but, as pointed out earlier, the hogging behaviour (in the context of multi-span continuous TCC floors) could well also be of interest. This means that the concrete, steel and timber could all

experience tensile and compressive stresses which place all these materials well into their nonlinear regimes of behaviour. Hence, in the next section of this report, the nonlinear constitutive models for the different materials are presented.

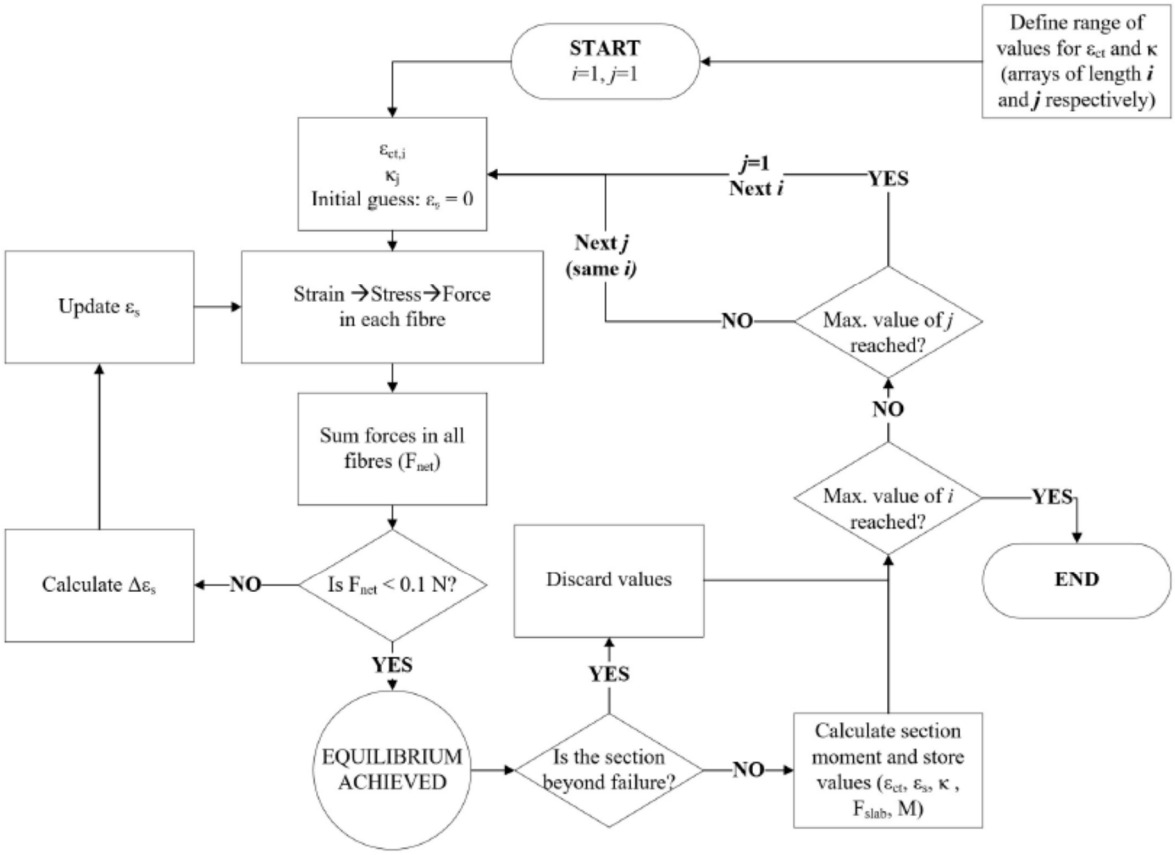

Fig. 2 – Flowchart for Computational Scheme

4 – Material Constitutive Behaviours

Concrete in tension was assumed to behave linearly elastically until cracking, with the stress dropping to zero for strains exceeding the cracking strain. In compression, the following EC2 [11] expression was used for concrete, namely:

$$\sigma_c(\varepsilon_c) = f_{cm} \cdot \frac{k \cdot \left(\varepsilon_c / \varepsilon_{c1}\right) - \left(\varepsilon_c / \varepsilon_{c1}\right)^2}{1 + (k-2) \cdot \left(\varepsilon_c / \varepsilon_{c1}\right)}$$ Eqn 7 ,

where f_{cm} is the mean cylinder compressive strength at 28 days, ε_{c1} is the strain at peak stress and the constant k is defined as follows :

$$k = 1.05 \cdot E_{cm} \cdot (\varepsilon_{c1}/f_{cm}) \qquad \text{Eqn 8 ,}$$

with E_{cm} being the secant modulus of elasticity between the unstressed state and the state at $0.4f_{cm}$. Eqn 7 is valid up to crushing of the concrete at strain ε_{cu1}. This stress-strain relationship is shown in Fig. 3.

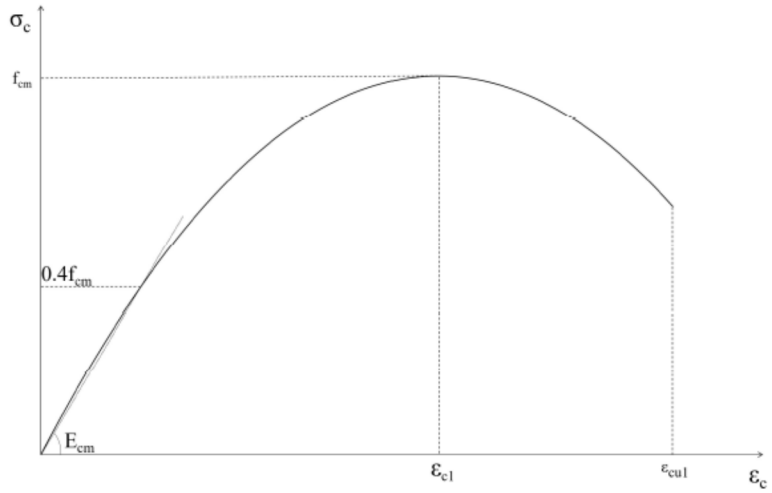

Fig. 3 – Assumed Uniaxial Compressive Stress-Strain Relation for Concrete

Timber in tension was assumed to be linear elastic up to fracture, but in compression to exhibit first linear elastic behaviour, followed by a nonlinear strain hardening behaviour before crushing. The model by Glos was used to capture these nonlinearities in the following form, namely :

$$\sigma(\varepsilon) = \frac{\varepsilon + \alpha_1 \cdot \varepsilon^n}{\alpha_2 + \alpha_3 \cdot \varepsilon + \alpha_4 \cdot \varepsilon^n} \qquad \text{Eqn 9 ,}$$

where the α constants are defined as :

$$\alpha_1 = \frac{100 \cdot f_{cy}}{(n-1) \cdot E_0 \cdot \varepsilon_{cu}^{(n-1)} \cdot (1 - f_{cy}/f_{cu})},\ \alpha_2 = \frac{1}{E_0},\ \alpha_3 = \frac{1}{f_{cu}} - \frac{n}{(n-1) \cdot E_0 \cdot \varepsilon_{cu}},\ \alpha_4 = \frac{\alpha_1}{f_{cy}}$$ Eqn 10,

where f_{cu} and ε_{cu} are the ultimate compressive stress and corresponding strain respectively, f_{cy} is a residual stress (typically $0.8f_{cu}$), E_0 is the tangent modulus (the same as the value for timber throughout its tension regime up to fracture) at zero strain and n is a shape parameter.

As shown later in this report, test data from Sebastian et al [9] were used to verify this computational framework. Comparison of the Glos model with the compressive stress-strain timber test data obtained in that study is shown in Fig. 4.

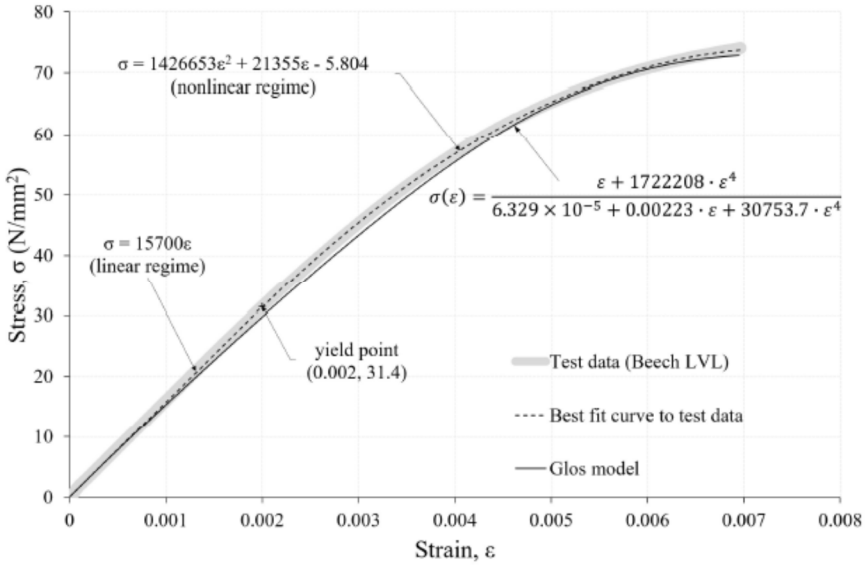

Fig. 4 – Uniaxial Compressive Stress-Strain Relation for Timber

Reinforcing steel was assumed to behave identically in tension and compression. Failing the provision of test data for such steel, the EC2 idealised model for such steel was used.

5 – Application of The Computational Scheme

The above computational scheme was verified using test data by Sebastian et al [9]. In that experimental study strain gauges were deliberately arranged to enable inference of joist curvature at different sections along the member, and to determine axial force (italicised *F* in the previous section) at these same timber sections, leading to the shear connection forces along short lengths of the TCC member.

5.1 – TCC Test Specimen Used for Verification

As shown in Fig. 5, the specimen was 4.8 m long and 2-span continuous including a short cantilever overhang vertically restrained at its tip. This rendered the specimen externally indeterminate in the longitudinal direction, so that it possessed both InI and LEI as defined in section 1 of this report. It also meant that both sagging and hogging moment developed at different locations along the member under the concentrated load applied at midspan of the longer of the two spans.

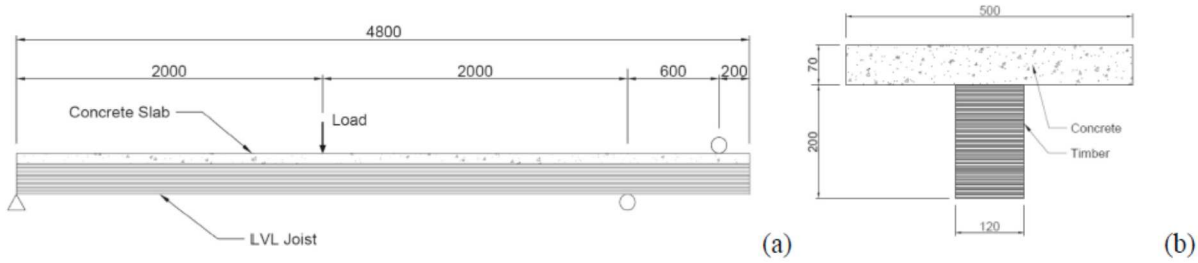

Fig. 5 – TCC Specimen Tested by Sebastian et al. [9] : (a) Elevation, (b) Section

Beech laminated veneer lumber, concrete grade C30/37, and five 12 mm diameter longitudinal steel reinforcing bars at 100 mm centres transversely with 20 mm cover from the top of the slab, were used. Table 1 gives the key material properties.

Material	Elastic Modulus (kN/mm^2)	Yield Stress (N/mm^2)	Ultimate Strength (N/mm^2)	Ultimate Strain
Timber (beech LVL)	15.7	31.4 (compression)	70	0.0070 (compression)
Concrete	32.8	-	30	0.0035 (compression)
Steel	187	281	372	0.025

Table 1 – Material Properties From Sebastian et al. [9]

5.2 – Unique Instrumentation Layout

As explained in Sebastian et al [9], there were three key features of the instrumentation layout which were deliberately designed in to enable inference of section behaviour. These were as follows, namely :

- Load cells were placed at the load points, the two support points and at the cantilever tip restraint point. This enabled the moment distribution along the specimen to be determined for any value of load applied to the specimen.
- Longitudinal strain gauges were placed along a vertical line near the top, mid-depth and base of the joist at various TCC sections. These gauges enabled through-depth strain distributions and so κ to be estimated for the joist sections.
- Directly above each gauged joist section, a longitudinal gauge was placed on the central steel reinforcing bar. This bar strain and an assumption of full slab-joist curvature compatibility enabled a through-depth strain distribution to be plotted for the slab.

Owing to this novel instrumentation layout, the through-depth strain distribution could be plotted for the entire depth of the TCC section, which in turn enabled both the slip strain (ε_s) and the strain at the top of the concrete slab (ε_{ct}) to be determined. Fig. 6 illustrates this use of the test data for one load applied to the TCC specimen. On this plot the black circles are the original strain gauge data, while the lines are the resulting through-depth strain distribution. The associated (k , ε_s , ε_{ct}) values derived from this exercise are written at the bottom right corner of the plot.

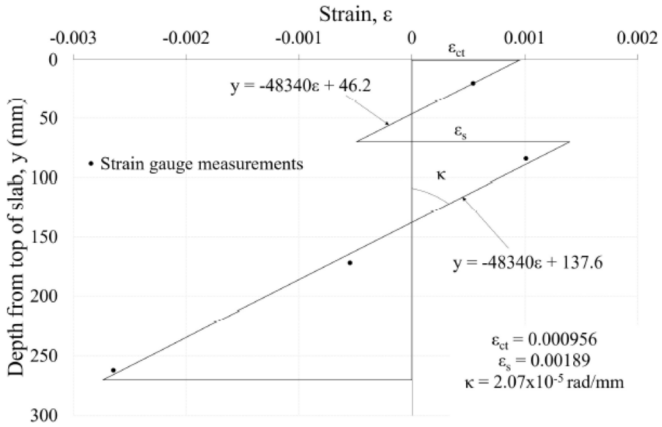

Fig. 6 – TCC Through-Depth Strain Distribution Derived From Test Data

5.3 – Verification of Computational Model

While the (M , κ , ε_s) and (F , κ , ε_s) surfaces have been under the spotlight thus far in this report, other surfaces, for example illustrating admissible (k , ε_s , ε_{ct}) sets may also be plotted. Since the (k , ε_s , ε_{ct}) sets readily emerge from processing of the test data, use of the corresponding surface is a useful way to illustrate the output from these computations and to illustrate levels of predictive-test agreement.

Thus, Fig. 7 shows the predicted (k , ε_s , ε_{ct}) surface along with corresponding test data shown as the thick black curves. Recall that both sag and hog moments developed in the TCC specimen, so that Fig. 7(a) shows the sag results and Fig. 7(b) the hog results. Each surface is shown from two different angles to facilitate visualisation. Two points readily emerge from the plots, namely that :

- In both cases the predicted vs test agreement is encouraging.
- The black curves lie in the lower regions of the surfaces, suggesting that the full capacities of neither the hog nor the sag sections of the specimen were approached during the testing. This provides a useful means of focusing on TCC **section** (as opposed to connection) behaviour for multi-span continuous TCCs.

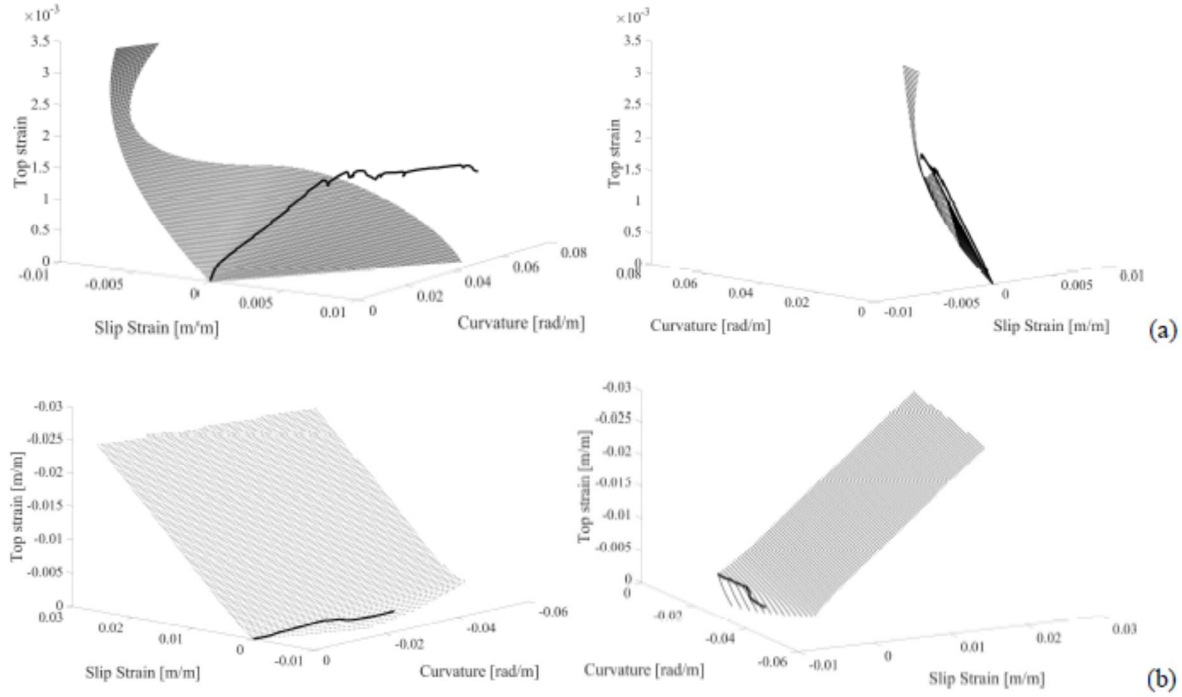

Fig. 7 – Predictive-Test Agreement for (k , ε_s , ε_{ct}) Surfaces : (a) Sag ; (b) Hog

This activation of only a small proportion of TCC capability is reinforced below. To that end, in addition to strain gauge readings, slip movement readings were also recorded at regular intervals along the TCC member. The resulting slip movement variations recorded along the member at three different loads are shown in Fig. 8.

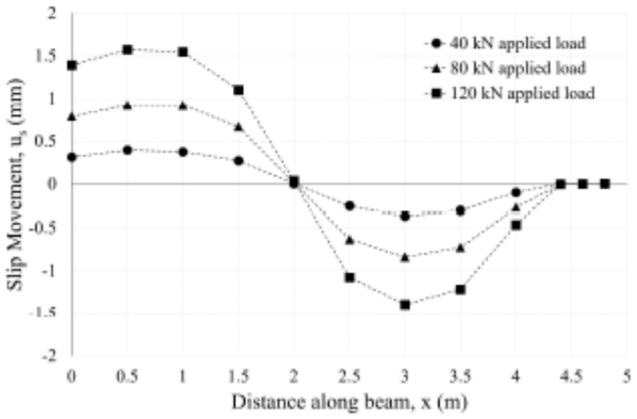

Fig. 8 – Slip Movement Profiles Recorded Along TCC Beam

For each slip profile, the gradients of lines between test data points gave slip strain estimates along the beam. Also, the shear force-slip curves for the slab-joist connections (from tests by Sebastian et al [9]) enabled the longitudinal shear forces in the connections along the beam to be estimated. Finally, by axial equilibrium, the sum of connector forces between the end of the beam and any section along the beam enabled the slab or joist axial force at that section to be estimated. So (F , ε_s) data sets were established for the TCC beam. Finally, the points on the (F , κ , ε_s) surface with these (F , ε_s) coordinates were located. The result is shown in Fig. 9.

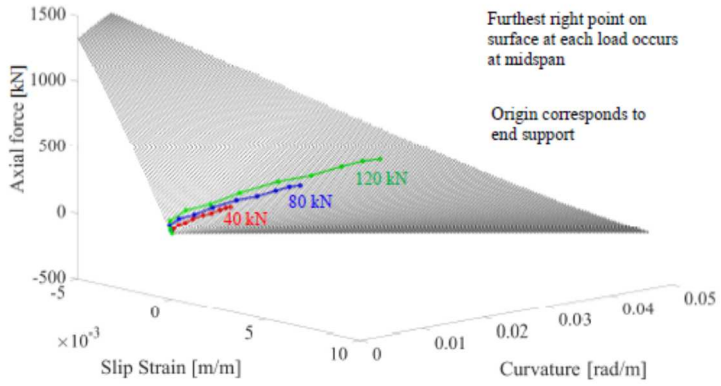

Fig. 9 – Trajectories on Sag Surface for Specimen by Sebastian et al [9]

That the trajectories (even at 120 kN, 71% of the failure load) lie in the lower reaches of the surface in Fig. 9 suggest low exploitation of TCC section capability.

5.4 – Section Flexural Characteristics : Moment and Deflection Predictions

The predicted (M , κ , ε_s) surface for the sag TCC section is shown in Fig. 10. Two edges of the surface define tensile fracture of the timber at the base of the section and crushing of the concrete at the top of the section as section failure modes.

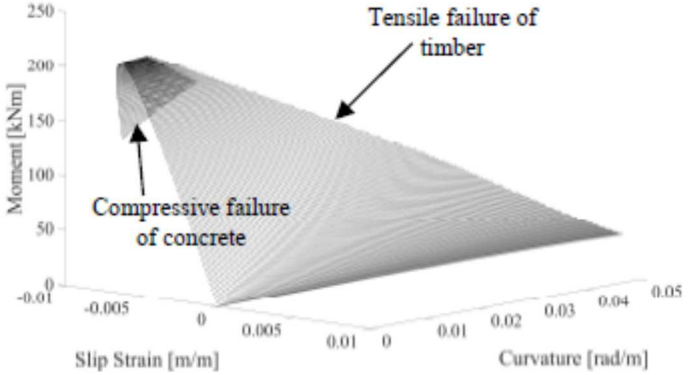

Fig. 10 – Sag (M , k , ε_s) Surface for TCC Section Tested by Sebastian et al. [9]

Using the test data on moments and corresponding slip strains along the TCC beam at different loads applied during the test, the corresponding curvatures were estimated from the surface of Fig. 10. Double integration of these along-beam κ profiles (area under the curve approximated as summed areas of small rectangles) was then used to estimate deflection at the centre of the main span. These deflections were then compared with the measured ones, with the result of Fig. 11.

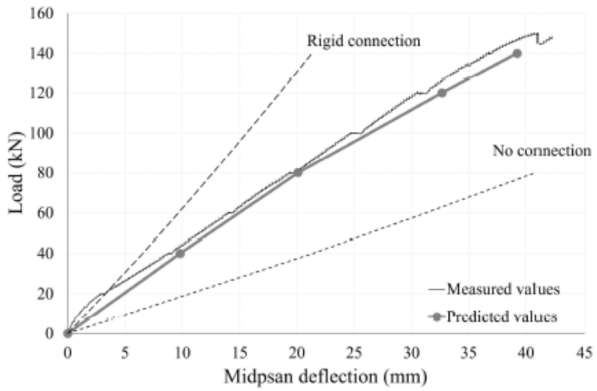

Fig. 11 – Midspan deflections for TCC Specimen of Sebastian et al. [9]

Note how the alternative assumptions of no connection and rigid connections lead to strong over- and under-estimates respectively of TCC deflection at midspan.

The associated TCC section *EI* profiles along the TCC beam, calculated as M/κ for three different loads applied to the beam are shown in Fig. 12. The drop in composite section flexural stiffness away from the end support is due to increased connection flexibility and higher stresses (thus lower stiffnesses of the materials on the TCC composite section. This is another useful output from the present theoretical framework, as such EI values can be fed into beam element computer analysis for prediction of TCC member behaviour under applied load.

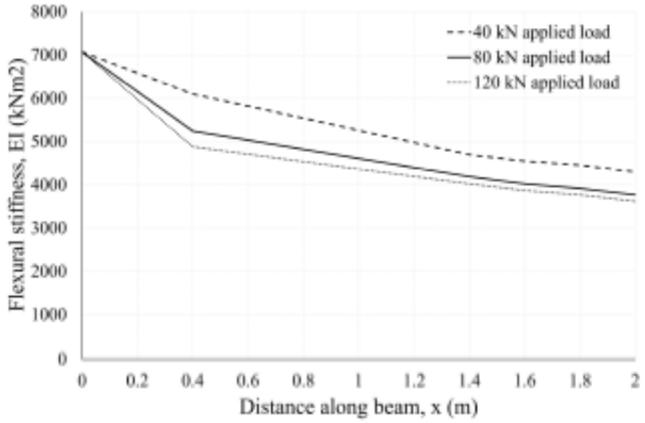

Fig. 12 – Predicted EI Profile Along TCC Beam at Different Applied Loads

Indeed, use of these *EI* profiles in beam element analysis led to good agreement with recorded data for midspan moment as a function of load, as shown in Fig. 13.

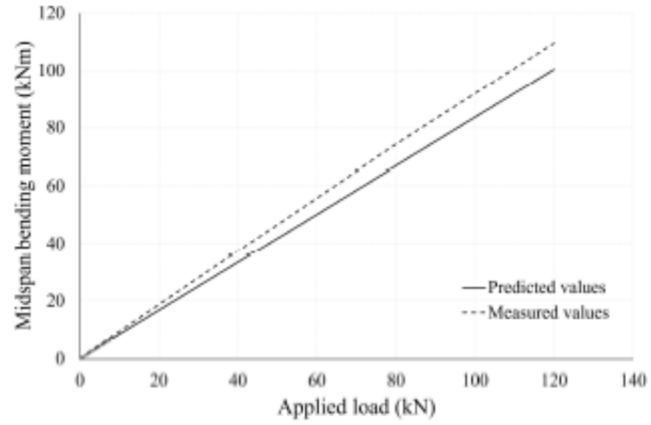

Fig. 13 – Predicted and Test-Inferred Midspan Moments

These results truly suggest the validity of the present theoretical framework.

6 – Conclusions and Future Work

From the presently conducted research, the following conclusions may be drawn :

- In a multi-span continuous timber-concrete composite (TCC) floor system, up to three levels of indeterminacy – internally due to slip, transversely due to multiple joists and longitudinally due to multi-span continuity – can exist. This dictates that quantifying the nonlinear TCC section stiffness profile throughout this structural system is crucial to predicting the load response.
- Hence in such TCC systems, as well as obtaining the constitutive behaviours of the timber-concrete connections, it is also important to characterise the constitutive behaviours of the TCC sections as entities in their own rights under both hog and sag curvatures.
- 3D surfaces linking various trio combinations of the composite section moment, curvature, slip strain, concrete top strain and slab or joist axial force, are novel, insightful and convenient ways of expressing these composite section constitutive behaviours.
- In this study, a novel computational framework has been developed to characterise these various surfaces. This computational framework uses a layered approach through the TCC section and nonlinear material constitutive models from the Eurocodes, with the effects in various layers linked by compatibility (including slip and curvature), and with the cumulative effects of the different layers used to give the overall TCC section characteristics.
- Collaborative testing (led by the author) was performed on a multi-span continuous TCC member including unique instrumentation layouts to permit reliable estimation of slip strain, TCC section curvature, section moment and slab or joist axial force. Via comparisons with the data from this testing, it has been shown that the present computational framework provides reliable descriptions of TCC section behaviour and leads to reliable prediction, via beam element (i.e. designer-friendly) analysis, of load response for ***multi-span continuous TCC members***. This is believed to be the first study of its kind.
- This computational framework shows great promise and must be advanced in future work to develop a designer-friendly yet reliable analysis scheme to predict the nonlinear load responses of TCC floors. This will encourage wide use of these low-weight, low-carbon, construction-friendly floor systems in practice.

Future research needed to build on the ideas contained in this report may be as follows, namely :

- Experimental and predictive studies of TCC floors which are both multi-span continuous longitudinally and comprise multiple longitudinal timber joists spaced at regular intervals transversely, with the slab transversely continuous across all joists.
- Consideration of prefabricated TCC floor panels which are then connected on site after having been craned into position.
- Establishing the influences of long-term effects on the M-κ-ε_s , F-κ-ε_s and other surfaces.
- Developing innovative analysis approaches to predict the nonlinear load responses of TCC floors, and defined by interaction between these novel constitutive surfaces for the TCC sections and the constitutive curves for the (including slab-joist) shear connections.

7 – Acknowledgements

The author expresses his sincere gratitude to the COST FP 1402 management team for enabling this STSM to collaborate with Professor Alfredo Dias. Further thanks are extended to Professor Dias for the fruitful exchange of ideas during the collaboration at the University of Coimbra. Finally, but by no means least, the author is also grateful to Mr Ollie Bell, MEng student at the University of Bristol, for using the computational scheme described in this report to generate the flowchart and results shown in Figs 2, 4, 7, and 9 – 13 of this report.

8 – References

[1] Ahmadi BH, Saka MP. Behaviour of Composite Timber-Concrete Floors. ASCE JSE, 1993, 119(11), 3111-30.

[2] Symons D. Design and Testing of a Composite Timber and Concrete Floor System. The Structural Engineer, 2006, 84(4), 22-30.

[3] Clouston P, Bathon LA, Schreyer A. Shear and Bending Performance of a Novel Wood-Concrete Composite System. ASCE JSE, 2005, 131(9), 1404-12.

[4] Gutkowski R, Brown K, Shigidi A, Natterer J. Laboratory Tests of Composite Wood-Concrete Beams. Construction and Building Materials, 2008, 22(6), 1059-66.

[5] Lukaszewska E, Fragiacomo M, Johnsson H. Laboratory Tests and Numerical Analyses of Pre-fabricated Timber-Concrete Composite Floors. ASCE JSE, 2010, 136(1), 46-55.

[6] Khorsandnia N, Valipor HR, Crews K. Experimental and Analytical Investigation of Short-Term Behaviour of LVL-Concrete Composite Connections and Beams. Constr. Bld Mat., 2012, 37, 229-38.

[7] Dias AMPG, Monteiro SRS, Martins CEJ. Reinforcement of Timber Floors – Transversal Load Distribution on Timber-Concrete Systems. Ed M. Piazza and M. Riggio, Advanced Materials Research, 2013, 778, 657-64.

[8] Kieslich H, Holschemacher K. Lateral Load Bearing Behavior of Timber-Concrete Composite Constructions. Ed M. Piazza and M. Riggio, Advanced Materials Research, 2013, 778, 665-72.

[9] Sebastian WM, Mudie J, Cox J, Piazza M, Tomasi R, Giongo I. Insight Into Mechanics of Externally Indeterminate Hardwood-Concrete Composite Beams. Construction and Building Materials, 2016, 102(2), 1029-48.

[10] European Committee for Standardisation (CEN) (2004a). Design of Timber Structures – Part 1 – 1: General – Common Rules and Rules for Buildings. Eurocode 5, Brussels, Belgium.

[11] Frangi A, Fontana M. Elasto-Plastic Model for Timber-Concrete Composite Beams with Ductile Connection. IABSE Str. Eng. Int., 2003, 13(1), 47-57.

9 – Appendix

Confirmation by the host institution of the successful execution of the STSM.

UNIVERSIDADE DE COIMBRA
FACULDADE DE CIÊNCIAS E TECNOLOGIA
DEPARTAMENTO DE ENGENHARIA CIVIL

Telefs:239797100/124
Fax: 239797123
E-Mail: decmail@dec.uc.pt

Alfredo Dias
Department of Civil Engineering
University of Coimbra

To whom it may concern

I hereby declare that the Short Term Scientific Mission (STSM) "Simplified Modelling for Multi-Span Continuous Timber-Concrete Composite Floors" proposed to the University of Coimbra, by Wendel Sebastian, Professor at Bristol University in the United Kingdom, was undertaken as planned between 13th and 27th March 2016. Furthermore, the presented report reflects the work undertaken as well as the common initiatives that will follow this STSM.

Coimbra 20 May 2016

Alfredo Manuel Pereira Geraldes Dias
(Host person for the STSM)